Science
May 2023, Volume 380 Issue 6647 Pages 812-817
https://doi.org/10.1126/science.abq4654
https://archimer.ifremer.fr/doc/00839/95132/

Natural iron fertilization by shallow hydrothermal sources fuels diazotroph blooms in the ocean

Bonnet Sophie [1, *], Guieu Cécile [2, *], Taillandier Vincent [2], Boulart Cedric [3], Bouruet-Aubertot Pascale [4], Gazeau Frédéric [2], Scalabrin Carla [5], Bressac Matthieu [2], Knapp Angela N. [6], Cuypers Yannis [4], González-Santana David [7, 8], Forrer Heather J. [6], Grisoni Jean-Michel [9], Grosso Olivier [1], Habasque Jeremie [7], Jardin-Camps Mercedes [1], Leblond Nathalie [9], Le Moigne Frédéric A. C. [1, 7], Lebourges-Dhaussy Anne [7], Lory Caroline [1], Nunige Sandra [1], Pulido-Villena Elvira [1], Rizzo Andrea L. [10, 11], Sarthou Geraldine [7], Tilliette Chloé [2]

[1] Aix Marseille University, Université de Toulon, CNRS, IRD, MIO Marseille, France.
[2] Laboratoire d'Océanographie de Villefranche (LOV), Institut de la Mer de Villefranche, CNRS, Sorbonne Université, 06230 Villefranche-sur-Mer, France.
[3] Adaptation et Diversité en Milieu Marin, UMR 7144 AD2M CNRS-Sorbonne Université, Station Biologique de Roscoff, 29680 Roscoff, France.
[4] Laboratoire d'Océanographie et du Climat: Expérimentation et Approches Numériques (LOCEAN-IPSL), Sorbonne University, CNRS-IRD-MNHN, 75005 Paris, France.
[5] Ifremer, Univ Brest, CNRS, UMR 6538 Geo-Ocean, F-29280 Plouzané, France.
[6] Department of Earth, Ocean, and Atmospheric Sciences, Florida State University, Tallahassee, FL 32306, USA.
[7] CNRS, Univ Brest, IRD, Ifremer, UMR 6539, LEMAR, Plouzané, France.
[8] Instituto de Oceanografía y Cambio Global (IOCAG), Universidad de Las Palmas de Gran Canaria, 35017 Las Palmas, Spain.
[9] Institut de la Mer de Villefranche, IMEV, Sorbonne Université, Villefranche-sur-Mer, France.
[10] Istituto Nazionale di Geofisica e Vulcanologia, Sezione di Milano, Via Alfonso Corti 12, 20133 Milano, Italy.
[11] Department of Earth and Environmental Sciences, University of Milano-Bicocca, Piazza della Scienza 4, 20126 Milan, Italy.

* Corresponding authors : Sophie Bonnet, email address : sophie.bonnet@mio.osupytheas.fr ; Cécile Guieu, email address : cecile.guieu@imev-mer.fr

Abstract :

Iron is an essential nutrient that regulates productivity in ~30% of the ocean. Compared with deep (>2000 meter) hydrothermal activity at mid-ocean ridges that provide iron to the ocean's interior, shallow (<500 meter) hydrothermal fluids are likely to influence the surface's ecosystem. However, their effect is unknown. In this work, we show that fluids emitted along the Tonga volcanic arc (South Pacific) have a substantial impact on iron concentrations in the photic layer through vertical diffusion. This enrichment stimulates biological activity, resulting in an extensive patch of chlorophyll (360,000 square kilometers). Diazotroph activity is two to eight times higher and carbon export fluxes are two to three times higher in

iron-enriched waters than in adjacent unfertilized waters. Such findings reveal a previously undescribed mechanism of natural iron fertilization in the ocean that fuels regional hotspot sinks for atmospheric CO_2 .

Planktonic diazotrophs are microscopic organisms ubiquitous in the ocean, that play a crucial role: they supply new available nitrogen (N) to the surface ocean biosphere, an essential but scarce nutrient in most of our oceans *(1, 2)*. Diazotrophs do so by converting atmospheric N_2 (endlessly available but metabolically useless) to ammonia (readily bioavailable), a reaction termed biological N_2 fixation. Diazotrophs thus alleviate N limitation in 60% of our oceans, especially in low latitudes, promoting CO_2 fixation by phytoplankton into organic carbon (primary productivity), that in turn, sustains the food web and organic carbon export and sequestration to the deep ocean (*3-6*). However, diazotrophs face a major challenge: besides phosphorus requirements, the iron (Fe)-rich nitrogenase enzyme that catalyzes N_2 fixation imposes a high Fe demand on diazotroph growth *(7)*, however Fe bioavailability in the ocean often limits the growth of these organisms *(6, 8)*. The Western subtropical South Pacific (WTSP) is a recognized hotspot of N_2 fixation activity, with an estimated contribution of ~21% to the global fixed N input *(9)*. Fe supply through atmospheric deposition is known to control large-scale diazotroph biogeography *(10)*, but such aeolian inputs are extremely low in this remote region *(11)*, suggesting the presence of alternative Fe fertilization processes underlying the ecological success of diazotrophs. Identifying these processes is of the utmost importance as diazotrophs have recently been identified as key drivers of future marine net primary productivity in response to climate change *(12)*. Here we demonstrate that Fe-rich fluids emitted by shallow hydrothermal venting directly fertilize the overlying surface ecosystem, inducing intense diazotroph activity supporting enhanced carbon export fluxes, with a C sequestration efficiency higher than those from artificial mesoscale Fe-addition experiments.

The WTSP hosts the Tonga-Kermadec subduction zone, stretching 2,500 km from New Zealand to Tonga (Fig. 1A). It is the fastest converging, most seismically active subduction zone, with the highest density of underwater volcanic centers on Earth *(13)*. This system produces extensive plumes of ^3He in the bathypelagic ocean (1500-2000 m) that fingerprint deep hydrothermal sources originating in the Lau basin *(14, 15)*. Other authors *(16, 17)* also identified shallower sources (<500 m) along the Tonga arc, associated with significantly elevated dissolved Fe (DFe) and manganese (DMn) concentrations close to the seafloor. Guieu et al. *(11)* demonstrated that these shallow sources were able to bring DFe up to the photic layer (~100 m) at high concentrations (up to 66 nmol $liter^{-1}$). These Fe infusions are hypothesized to fuel the observed N_2 fixation hot spot associated with an elevated chlorophyll (Chl) patch persisting 6 months per year in this region *(9, 11)* (Fig 2A,B). Yet, there is currently no empirical evidence of the direct effect of such hydrothermal Fe fertilization on the overlying planktonic ecosystem, with the implication that a significant part of new N entering the tropical Pacific -thanks to hydrothermal Fe- is likely missing from N budgets. Such an Fe supply mechanism would challenge the prevailing paradigm that diazotroph productivity is mainly mediated by Fe from dust deposition *(10)* in N-limited regions.

To document the mechanistic link between Fe supply from submarine volcanism and the response of the surface plankton community, we combine acoustic, chemical, physical, and biological data acquired during the GEOTRACES GPpr14 TONGA expedition *(18)*, a zonal transect between the Tonga volcanic arc and the South Pacific Gyre, which serves as a reference deep-sea site where the ocean surface is not impacted by hydrothermal activity. The targeted submarine volcano (Volcano #1 *(16, 17)*) is a large stratovolcano (basal diameter 28 km) located in the central part of the Tonga arc (-21.154 ; -175.744) (Fig. 1A, B). During an acoustic survey above the volcano, we detected multiple acoustic plumes (Fig. 1B, Table S1) rising from the sea floor up to ~20 m below the surface ocean (Fig. 1C). We focused our study on a site located near the caldera on the southwestern edge of the volcano (Fig. 1B) (hereafter referred

to as 'Panamax site'), where the acoustic anomaly *(19-21)*, also associated with intense gas bubble emissions, was strong and continuous (Fig. 1D). Repeated CTD casts at this site revealed that acoustic plumes were also associated with strong anomalies in pH, turbidity, and redox potential (Eh) (Fig. 1E, Table S2) from the seafloor (195 m depth) up to ~160 m. Methane concentrations that reached >100 nmol liter^{-1} (Fig. 1F) and the excess of ^{3}He and ^{4}He concentrations (Fig. S1) confirmed the hydrothermal origin of the plumes.

DFe and DMn were also enriched ~80-fold at this site (Fig. 1F) compared to similar depths in the WTSP *(11, 22)*. DFe and CH_4 concentrations were positively correlated (R^2=0.89, p<0.05). DFe reached concentrations as high as 48.5 nmol liter^{-1} at 195 m (within the main acoustic signal), and although they decreased towards the photic layer (~0-100 m), DFe concentrations in that layer (~0.6 to 10 nmol liter^{-1}) (Fig. 1F) were one order of magnitude higher compared to those at stations not impacted by hydrothermal activity *(23)*. The turbulence profiles (Fig. S2) revealed an order of magnitude higher vertical diffusivity above the volcano (Kz = 3.7±1.9x10^{-5} m^2 s^{-1} at ~50 m, corresponding to the base of the surface mixed layer) compared to the distal open-sea reference site (Kz = 5.2±9.6x10^{-6} m^2 s^{-1}) (Table 1), in line with previous work above shallow (~200 m) seamounts (*24*). Combining the measured Kz with the DFe gradients (Table 1 and Supplementary materials), the diffusive DFe vertical supply to the mixed layer above the volcano reached 1.1±1.7x10^{-4} mmol Fe m^{-2} d^{-1}. This is orders of magnitude larger than at the reference site (Table 1), suggesting that Fe-rich fluids released close to the shallow volcano represent a significant Fe source to surface waters. A phosphate supply of 5.4±2.4x10^{-3} mmol m^{-2} d^{-1} accompanied this vertical DFe supply, while no nitrate supply could be quantified (Table S4) due to the decoupling between the depth of the phosphacline (~50 m) and the nitracline (~100 m) (Fig. S5), as already observed in the WTSP (*25*).

Along the west to east zonal transect, total chlorophyll-a (Chl*a)* and particulate organic N stocks peaked in the naturally Fe-fertilized waters at Volcano #1 (Fig. 2). Both were also elevated up and downstream of the arc (Fig. 2C) consistent with ocean color images (Fig. 2A). This biomass peak was associated with 2 to 8-fold enhanced N_2 fixation rates relative to surrounding waters on either side of the arc (p<0.05, Mann-Whitney test) (Fig 2E), and 90-fold higher *Trichodesmium* spp. abundances (p<0.05, Mann-Whitney test) (Fig. 2F). This led to extremely high N_2 fixation rates and *Trichodesmium* spp. abundances in the Fe-fertilized waters (>2000 µmol N m^{-2} d^{-1} ; ~6 x 10^7 *nifH* copies L^{-1}), i.e. one to two orders of magnitude greater than values commonly found in other (sub)tropical ocean basins (*26*). This peak in diazotroph activity was marked by a phosphate drawdown (~50 nM) in the photic layer, although concentrations were not limiting for *Trichodesmium* spp. *(27)* due to intense microbial phosphorus cycling in this region *(28)*. Diazotrophs were favored by the extremely low nitrate concentrations along the transect (Fig. S6).

The particulate organic carbon (POC) and nitrogen (PON) export fluxes were measured using surface tethered sediment traps deployed for 4 days near Volcano #1 and at the reference site. Consistent with model simulations in this region *(22)*, POC export at 170 m and 270 m was 2 to 3 times higher in the Fe-fertilized patch than at the reference site (Table 1), resulting in an excess of POC export of 1.5 to 2.5 mmol C m^{-2} d^{-1} in the fertilized waters. Comparing measurements of subsurface water column nitrate+nitrite δ^{15}N (1.2 to 2.2‰) with the δ^{15}N of sinking PON (-0.5± 3.5‰ at 170 m and -0.2± 1.9‰ at 270 m, respectively), the N isotope budget (N_2 fixation end member = -1‰) revealed that N_2 fixation supported 77 to 84±159% at 170 m and 64 to 75±86% at 270 m of the export production in the Fe-fertilized area, consistent with the massive export of diazotrophs observed in the traps during the expedition *(3, 29)*. Collectively, these results suggest that the hydrothermally-driven Fe fertilization fuels

planktonic diazotrophs, resulting in low $\delta^{15}N$ of sinking PON and high POC export fluxes compared to subtropical systems not impacted by hydrothermal activity *(30)* (Table S5).

To confirm the causal link between hydrothermal inputs and diazotroph activity, we conducted novel experiments where hydrothermally-enriched waters collected at the 'Panamax site' of Volcano #1 (hereafter referred to as 'plume water') were supplied to surface biological communities using 300-L trace metal clean reactors (Fig. S7A, Methods). Increasing plume water volumes (from 0 to 14.5% of the total reactors volume) were added to surface seawater from outside of the direct volcanic influence (-21.683°N ; -174.709°E). The plume water was characterized by low pH (6.4) compared to ambient seawater (8.1) and DFe concentrations (15.8 nmol liter^{-1}) were ~15-fold higher than in ambient surface waters (1.0 nmol liter^{-1}) (Table S6). The increasing additions resulted in consistent increases of DFe concentrations and decreasing pH in the experimental reactors (Fig. S7). Plume water additions enhanced N_2 fixation rates by a factor of 7 to 8 on average over all sampling days compared to those measured in the unamended control ($p<0.05$, Mann-Whitney test) (Fig. 3A), reaching levels in the same range as *in situ* rates measured above the volcano (Fig. 2E). Likewise, as observed *in-situ*, *Trichodesmium* abundances increased by a factor of 3 to 5-fold ($p<0.05$, Mann-Whitney test) in plume water-amended reactors (Fig. 3B). Both N_2 fixation rates and *Trichodesmium* abundances decreased at the end of the experiment, likely as a consequence of phosphate depletion in the closed reactors (no possible turbulent diffusion) (Fig. S7), but generally remained higher in the amended reactors compared to those measured in the control. Due to the low inorganic N:P molar ratio (~9:1) in the plume water (indicative of a greater phosphate availability relative to nitrate), the mixing of the plume water with surface seawater likely prevented the phosphate limitation for up to days 6-8, while nitrate was depleted after 2 days. This decoupling between nitrate and phosphate also mirrors the *in situ* data described above.

The Fe supply from the Tonga arc thus drives in large part upper ocean phenology of biological activity. We estimate that the region of elevated Chl*a* extends ~800 km in longitude and ~450 km in latitude (Fig. 1A), forming a hot spot of biological activity of ~360,000 km^2 in the middle of the otherwise desert-like WTSP. The trajectories of SVP (surface velocity program) drifters deployed above Volcano #1 indicate that over a 6-month period, Fe-fertilized water masses can be dispersed regionally and support this extended Chl*a* patch (Fig. S8). The trajectories provide a bulk representation of complex dynamical processes occurring at smaller scales, involving the South Equatorial current and modulated by mesoscale activity *(11, 31)*, or lateral stirring by filaments *(32)*. In addition, multiple active vent fields have been (recently) identified along the Tonga arc and the Lau Basin *(16, 17, 33, 34)*, either at shallow depths (<500 m) or deeper (500-1000 m). Although all active shallow vents have not yet been discovered, with a density estimation of one active volcano center per 12 km of arc, fertilization processes such as those evidenced at Volcano #1 likely occur at many locations along the arc, further explaining the regional extent of the Chl*a* patch observed by satellite (Fig. 2A). We cannot exclude that the few emerged Tonga islands could provide additional nutrients, likely contributing to the observed bloom. However, a study conducted over the entire tropical Pacific reveals that these island mass effects are generally very localized (around the islands, with a Chl*a* patch area of 9-13 km^2) and are of moderate amplitude (+9% of Chl*a* increase relative to background waters) *(35)*. In contrast, the bloom in the region of the Tonga volcanic arc is unique in that it is much larger (360,000 km^2) and of greater amplitude (~100% Chl*a* increase) than around any other Pacific islands/archipelagos. This means that additional Fe sources of hydrothermal origin are necessary to sustain such a bloom. As an example, very weak Chl*a* is observed around the Cook Islands located at the same latitude as Tonga, receiving the same amount of rainfall and aerosol-Fe deposition annually, but not impacted by hydrothermal activity (Fig. S9), confirming that

nutrients of terrestrial origin are not sufficient to sustain blooms of large amplitude. Finally, some extremely rare events such as the massive eruption of the Hunga Tonga Hunga Ha'apai volcano in January 2022 could also cause short-term localized blooms, such as the one observed from satellite following the eruption *(36)*, that had no visible effect on the interannual trend of Chl*a*. Other authors suggest that the interpretation of the Chl*a* increase after the eruption was distorted by the presence of abundant volcanic particles suspended in the water column following the eruption *(37)*.

Looking more deeply into the 25-year monthly Chl*a* time series (Fig. 2B, S10), we find that, despite interannual variability, the bloom develops every year for at least 6 months in austral summer. This seasonal characteristic is probably linked to the thermal fitness of *Trichodesmium*, who are thought to only bloom at temperatures >25°C -reached in the WTSP between November and April (austral summer)-. This thermal constraint for *Trichodesmium* also probably explains why the bloom does not extend south of ~23°S, which marks the location of the 25°C isotherm. Further south, surface waters are also depleted in nitrate, and in the absence of diazotrophs, the new Fe supplied by hydrothermal vents along the arc cannot be taken up to produce new biomass. As models predict a sea surface temperature increase of 1.5°C by the end of the century in the Tonga arc region (*38*), it is possible that the thermal constraint for diazotrophs will be relieved and the bloom will spread further south in the future.

To properly account for the seasonal variability of export, we deployed a moored sediment trap at 1000 m for a full annual cycle in the fertilized patch (see SI). We show that POC export was 5 times higher in austral summer compared to winter (Fig. 4), resulting in a seasonally-integrated (6 summer months) POC export of 74 mmol C m^{-2}, i.e. 80% of the annual POC export flux. The low $\delta^{15}N$ signature of sinking PON during these summer months (~0-1‰) confirms that N_2 fixation supports most export production during that season. In austral winter, the higher sinking PON $\delta^{15}N$ values (2-8‰) suggest that other N sources (i.e., deep nitrate) fuel the low export production. For comparison, the annual POC flux measured here in the subtropical ocean is of the same order of magnitude as that measured in the Southern Ocean in naturally Fe-fertilized waters (*39, 40*). This suggests that Fe-fertilized regions of the oligotrophic ocean can act as net CO_2 sinks, provided sufficient phosphorus availability. The Fe-fertilized WTSP is a unique ecosystem allowing C sequestration supported by N_2 fixation due to substantial winter phosphate replenishment (not associated with nitrate supply due to decoupling of phosphacline and nitracline depths) (*25*) and to a turbulent diffusive flux of Fe and phosphate (19 mmol : mol^{-1}) meeting *Trichodesmium* requirements (*41*). Furthermore, *Trichodesmium* can reduce its P quotas under P stress (*42, 43*), and actively utilizes dissolved organic P (DOP) compounds in this region (*44*), likely enhanced by high Fe availability (*45*). Taken together, this suggests that P and Fe work in concert to trigger extensive diazotroph blooms and C sequestration by N_2-based new production in the WTSP.

Compared to shelf-driven natural Fe fertilizations occurring in HNLC (High Nutrient, Low Chlorophyll) waters of the Southern Ocean (SO), the TONGA bloom is generally more temporally and spatially extensive, despite its lower intensity (depth integrated Chl*a*) (Table 1) *(39, 46-48)*. The total DFe flux in this study (130 nmol Fe m^{-2} d^{-1}) was generally lower than that measured in Fe-enriched waters downstream of the Kerguelen plateau (KEOPS cruise in 2005, 222 nmol Fe m^{-2} d^{-1} *(49)*) and downstream of the Crozet plateau (CROZEX cruise in 2004, 550 nmol Fe m^{-2} d^{-1} *(39)*) (Table 1). However, unlike HNLC regions, surface waters of the WTSP are nitrate-depleted, and only N_2-fixing organisms can exploit this new Fe to build biomass and drive carbon export to the deep ocean, as long as sufficient phosphorus remains available. Based on the excess POC export and the excess of DFe supply at the time of the

cruise (Table 1), we calculated a C sequestration efficiency (defined as the ratio of the excess POC export to the amount of excess DFe supplied) of 13600 and 23000 mol C mol^{-1} Fe (at 170 and 270 m, respectively). Although comparisons between studies need to be considered with caution given the different methods used and timescales considered to estimate both excess Fe supply and POC export, this sequestration efficiency is higher than those from artificial mesoscale Fe-addition experiments (e.g. 4300 mol mol^{-1} for SOFeX *(50)*; 1200 mol mol^{-1} for SERIES *(51)*), and in the range of values measured in naturally-fertilized HNLC regions (8600 mol mol^{-1} for CROZEX *(39)* to 154,000 mol mol^{-1} during KEOPS *(49)*). This confirms that natural Fe fertilizations are more efficient for carbon sequestration than purposeful Fe additions. In addition, comparing such estimates from various natural oceanic settings, Le Moigne et al. *(52)* suggested that the apparent variability in C sequestration efficiency may be related to the timescale of Fe delivery (slow delivery being more efficient). Therefore, attention must be paid in future studies to the timescale of delivery of this newly-recognized mode of Fe supply through shallow hydrothermalism, including in temperate and polar ecosystems, where this efficiency could be even more important due to higher macronutrient availability.

Our conceptual view of the ocean Fe cycle has greatly evolved over the past 10 years, highlighting the importance of hydrothermal activity on the Fe cycle *(53)*. While model simulations suggest that hydrothermal inputs associated with mid-ocean ridges (>2000 m) contribute 23% of the Fe found in the global ocean water column, that Fe only directly supports 3% of carbon export at 100 m *(54)*. This is mostly because a large part of that Fe remains in the deep ocean over long time scales *(53)* and needs to be entrained in surface waters before potentially impacting photosynthetic communities *(46, 48)*. Fe from intermediate depth (~1000 m) vents may also be transported long distances and with the condition that these waters upwell, influence marine ecosystems located thousands of km far from the site of discharge *(55)*. However, hydrothermal venting also occurs at shallower depths (<500 m) in island arc systems such as the Tonga arc. Even if scavenging and precipitation removes part of this newly-emitted Fe from the dissolved pool *(23)*, such shallow sources can supply Fe rapidly to overlying surface photosynthetic communities compared to Fe emitted deeper *(23, 55)*. In the oligotrophic ocean, the implications of such shallow hydrothermal Fe fertilization are highly significant as they directly fuel surface diazotrophs and export of organic matter to the deep ocean, representing regional hotspot sinks of atmospheric CO_2. We demonstrate here that shallow hydrothermal sources also represent a triggering factor on diazotroph blooms in regions where the atmospheric supply of DFe is virtually absent. Such forcing is of the utmost importance to study as climate models predict an expansion of the oligotrophic gyres (40% of our oceans) *(56)* where diazotrophs will likely thrive. Furthermore, in a warmer, more stratified ocean, such shallow Fe sources are likely to deliver Fe to surface communities more readily than deep sources *(55)*. Beyond the oligotrophic oceans, shallow hydrothermal fertilizations are likely to be common in the global ocean, due to the high number of shallow hydrothermal vents associated with island arc systems and submarine volcanic calderas (*57*) whose exact number/locations are still yet to be discovered *(14)*. Such systems are also present at higher latitudes, notably in the HNLC waters in the subarctic Pacific and the SO *(57)*. Therefore, a comprehensive evaluation of their impact in these severely Fe-limited systems where surface mixed layers reach the intermediate or even the deep ocean water masses is clearly needed. Finally, the extent to which such hydrothermal-driven biological carbon pump enhancement may have changed atmospheric CO_2 in the past remains unclear. Future studies would be relevant as the hydrothermal flux of Fe has been relatively constant over millennial timescales *(58)*.

References and Notes

1. C. M. Moore *et al.*, Processes and patterns of oceanic nutrient limitation. *Nature Geoscience* **6**, 701–710 (2013).
2. N. Gruber, in *Nitrogen in the marine environment*. (2008), pp. 1-50.
3. S. Bonnet *et al.*, Diazotrophs are overlooked contributors to carbon and nitrogen export to the deep ocean. *The ISME journal* **17**, 47-58 (2022).
4. D. M. Karl, M. J. Church, J. E. Dore, R. Letelier, C. Mahaffey, Predictable and efficient carbon sequestration in the North Pacific Ocean supported by symbiotic nitrogen fixation. *Proceedings of the National Academy of Sciences* **109**, 1842–1849 (2012).
5. A. Subramaniam *et al.*, Amazon River enhances diazotrophy and carbon sequestration in the tropical North Atlantic Ocean. *Proceedings of the National Academy of Sciences* **105**, 10460–10465 (2008).
6. J. P. Zehr, D. G. Capone, Changing perspectives in marine nitrogen fixation. *Science* **368**, (2020).
7. C. Lory *et al.*, Assessing the contribution of diazotrophs to microbial Fe uptake using a group specific approach in the Western Tropical South Pacific Ocean. *ISME Communications* **2**, 1-11 (2022).
8. J. A. Sohm, E. A. Webb, D. G. Capone, Emerging patterns of marine nitrogen fixation. *Nature Reviews Microbiology* **9**, 499-508 (2011).
9. S. Bonnet, M. Caffin, H. Berthelot, T. Moutin, Hot spot of N2 fixation in the western tropical South Pacific pleads for a spatial decoupling between N2 fixation and denitrification. *Proceedings of the National Academy of Sciences* **114**, E2800-E2801 (2017).
10. C. Schlosser *et al.*, Seasonal ITCZ migration dynamically controls the location of the (sub)tropical Atlantic biogeochemical divide. *Proceedings of the National Academy of Sciences of the United States of America* **111**, 1438-1442 (2014).
11. C. Guieu *et al.*, Iron from a submarine source impacts the productive layer of the Western Tropical South Pacific (WTSP). *Scientific Reports* **8**, 9075 (2018).
12. L. Bopp *et al.*, Diazotrophy as a key driver of the response of marine net primary productivity to climate change. *Biogeosciences* **19**, 4267-4285 (2022).
13. C. E. J. de Ronde *et al.*, in *Volcanic, Geothermal, and Ore-Forming Fluids: Rulers and Witnesses of Processes within the Earth*. (Society of Economic Geologists, 2005), vol. 10, pp. 0.
14. C. R. German *et al.*, Hydrothermal impacts on trace element and isotope ocean biogeochemistry. *Phil. Trans. R. Soc. A* **374**, 20160035 (2016).
15. J. E. Lupton, D. G. Pyle, W. J. Jenkins, R. Greene, L. Evans, Evidence for an extensive hydrothermal plume in the Tonga-Fiji region of the South Pacific. *Geochem Geophy Geosy* **5**, (2004).
16. P. Stoffers *et al.*, Submarine volcanoes and high-temperature hydrothermal venting on the Tonga arc, southwest Pacific. *Geology* **34**, 453-456 (2006).
17. G. Massoth *et al.*, Multiple hydrothermal sources along the south Tonga arc and Valu Fa Ridge. *Geochemistry, Geophysics, Geosystems* **8**, (2007).
18. C. Guieu, S. Bonnet, TONGA GEOTRACES GPpr14 ocean expedition, https://doi.org/10.17600/18000884. (2019).
19. C. Boulart *et al.*, Active hydrothermal vents in the Woodlark Basin may act as dispersing centres for hydrothermal fauna. *Commun Earth Environ* **3**, (2022).
20. W. W. Chadwick *et al.*, Imaging of CO2 bubble plumes above an erupting submarine volcano, NW Rota-1, Mariana Arc. *Geochem Geophy Geosy* **15**, 4325-4342 (2014).
21. N. Feuillet *et al.*, Birth of a large volcanic edifice offshore Mayotte via lithosphere-scale dyke intrusion. *Nature Geoscience* **14**, 787-+ (2021).

22. J. A. Resing *et al.*, Basin-scale transport of hydrothermal dissolved metals across the South Pacific Ocean. *Nature* **523**, 200-203 (2015).
23. C. Tilliette *et al.*, Dissolved Iron Patterns Impacted by Shallow Hydrothermal Sources Along a Transect Through the Tonga-Kermadec Arc. *Global Biogeochemical Cycles* **36**, e2022GB007363 (2022).
24. J. Lavelle, I. Lozovatsky, D. Smith IV, Tidally induced turbulent mixing at Irving Seamount—modeling and measurements. *Geophysical research letters* **31**, (2004).
25. T. Moutin *et al.*, Nutrient availability and the ultimate control of the biological carbon pump in the western tropical South Pacific Ocean. *Biogeosciences* **15**, 2961-2989 (2018).
26. Y.-W. Luo *et al.*, Database of diazotrophs in global ocean: abundance, biomass and nitrogen fixation rates. *Earth System Science Data* **4**, 47-73 (2012).
27. A. Filella *et al.*, Contrasting Roles of DOP as a Source of Phosphorus and Energy for Marine Diazotrophs. *Frontiers in Marine Science* **9**, (2022).
28. F. Van Wambeke *et al.*, Dynamics and controls of heterotrophic prokaryotic production in the western tropical South Pacific Ocean: links with diazotrophic and photosynthetic activity. *Biogeosciences* **15**, 2669-2689 (2018).
29. M. Benavides *et al.*, Sinking Trichodesmium fixes nitrogen in the dark ocean. *The ISME journal* **16**, 2398-2405 (2022).
30. A. N. Knapp *et al.*, Distribution and rates of nitrogen fixation in the western tropical South Pacific Ocean constrained by nitrogen isotope budgets. *Biogeosciences* **15**, 2619-2628 (2018).
31. L. Rousselet *et al.*, Large- to submesoscale surface circulation and its implications on biogeochemical/biological horizontal distributions during the OUTPACE cruise (southwest Pacific). *Biogeosciences* **15**, 2411-2431 (2018).
32. A. de Verneil, L. Rousselet, A. M. Doglioli, A. A. Petrenko, T. Moutin, The fate of a southwest Pacific bloom: gauging the impact of submesoscale vs. mesoscale circulation on biological gradients in the subtropics. *Biogeosciences* **14**, 3471-3486 (2017).
33. S. E. Beaulieu, E. T. Baker, C. R. German, A. Maffei, An authoritative global database for active submarine hydrothermal vent fields. *Geochem Geophy Geosy* **14**, 4892-4905 (2013).
34. C. R. German *et al.*, Hydrothermal impacts on trace element and isotope ocean biogeochemistry. *Philosophical Transactions of the Royal Society A: Mathematical, Physical and Engineering Sciences* **374**, (2016).
35. M. Messie, A. Petrenko, A. M. Doglioli, E. Martinez, S. Alvain, Basin-scale biogeochemical and ecological impacts of islands in the tropical Pacific Ocean. *Nature Geoscience* **15**, 469-+ (2022).
36. B. Barone, R. M. Letelier, K. H. Rubin, D. M. Karl, Satellite Detection of a Massive Phytoplankton Bloom Following the 2022 Submarine Eruption of the Hunga Tonga-Hunga Ha‘apai Volcano. *Geophysical Research Letters* **49**, e2022GL099293 (2022).
37. A. Whiteside *et al.*, Impact of ashes from the 2022 Tonga volcanic eruption on satellite ocean color signatures. *Frontiers in Marine Science* **9**, (2023).
38. L. Dhage, M. J. Widlansky, Assessment of 21st Century Changing Sea Surface Temperature, Rainfall, and Sea Surface Height Patterns in the Tropical Pacific Islands Using CMIP6 Greenhouse Warming Projections. *Earths Future* **10**, (2022).
39. R. T. Pollard *et al.*, Southern Ocean deep-water carbon export enhanced by natural iron fertilization. *Nature* **457**, 577-580 (2009).
40. M. Rembauville, I. Salter, N. Leblond, A. Gueneugues, S. Blain, Export fluxes in a naturally iron-fertilized area of the Southern Ocean - Part 1: Seasonal dynamics of

particulate organic carbon export from a moored sediment trap. *Biogeosciences* **12**, 3153-3170 (2015).
41. J. Nuester, S. Vogt, M. Newville, A. B. Kustka, B. S. Twining, The unique biogeochemical signature of the marine diazotroph trichodesmium. *Frontiers in microbiology* **3**, 150 (2012).
42. D. M. Karl, R. Letelier, D. V. Hebel, D. F. Bird, C. D. Winn, *Trichodesmium blooms and new nitrogen in the North Pacific Gyre*. C. D. G. R. J. G. Carpenter E.J., Ed., Marine pelagic cyanobacteria:Trichodesmiurn and other diazotrophs. (Kluwer Academic Publishers, Dordrecht, 1992), pp. 219-237.
43. A. E. White, Y. H. Spitz, D. M. Karl, R. M. Letelier, Flexible elemental stoichiometry in Trichodesmium spp. and its ecological implications. *Limnology and Oceanography* **51**, 1777-1790 (2006).
44. Z. Liang, R. T. Letscher, A. N. Knapp, Dissolved organic phosphorus concentrations in the surface ocean controlled by both phosphate and iron stress. *Nature Geoscience* **15**, 651-+ (2022).
45. T. J. Browning *et al.*, Iron limitation of microbial phosphorus acquisition in the tropical North Atlantic. *Nature Communications* **8**, (2017).
46. M. Ardyna *et al.*, Hydrothermal vents trigger massive phytoplankton blooms in the Southern Ocean. *Nat Commun* **10**, 2451 (2019).
47. S. Blain, S. Bonnet, C. Guieu, Dissolved iron distribution in the tropical and sub tropical South Eastern Pacific. *Biogeosciences* **5**, 269–280 (2008).
48. C. M. S. Schine *et al.*, Massive Southern Ocean phytoplankton bloom fed by iron of possible hydrothermal origin. *Nat Commun* **12**, 1211 (2021).
49. S. Blain *et al.*, Effect of natural iron fertilization on carbon sequestration in the Southern Ocean. *Nature* **446**, 1070-1074 (2007).
50. K. O. Buesseler, J. E. Andrews, S. M. Pike, M. A. Charette, The effect of iron fertilization on carbon sequestration in the Southern ocean. *Science* **304**, 414-417 (2004).
51. P. W. Boyd *et al.*, The decline and fate of an iron-induced subarctic phytoplankton bloom. *Nature* **428**, 549-553 (2004).
52. F. A. C. Le Moigne *et al.*, Sequestration efficiency in the iron-limited North Atlantic: Implications for iron supply mode to fertilized blooms. *Geophysical Research Letters* **41**, 4619-4627 (2014).
53. A. Tagliabue *et al.*, The integral role of iron in ocean biogeochemistry. *Nature* **543**, 51-59 (2017).
54. A. Tagliabue, O. Aumont, L. Bopp, The impact of different external sources of iron on the global carbon cycle. *Geophysical Research Letters* **41**, 920-926 (2014).
55. W. Jenkins *et al.*, An intermediate-depth source of hydrothermal 3He and dissolved iron in the North Pacific. *Earth and Planetary Science Letters* **539**, 116223 (2020).
56. J. J. Polovina, E. A. Howell, M. Abecassis, Ocean's least productive waters are expanding. *Geophysical Research Letters* **35**, (2008).
57. J. A. Hawkes, D. P. Connelly, M. J. A. Rijkenberg, E. P. Achterberg, The importance of shallow hydrothermal island arc systems in ocean biogeochemistry. *Journal of Geophysical Research*, (2014).
58. N.-C. Chu *et al.*, Evidence for hydrothermal venting in Fe isotope compositions of the deep Pacific Ocean through time. *Earth and Planetary Science Letters* **245**, 202-217 (2006).
59. W. W. Chadwick et al., Imaging of CO2 bubble plumes above an erupting submarine volcano, NW Rota-1, Mariana Arc. Geochem Geophy Geosy 15, 4325-4342 (2014).
60. J. M. Augustin, 2023. SonarScope software. SEANOE. https://doi.org/10.17882/87777.

61. C. B. Poncelet, G., Corre, M.P. (2023). Globe (GLobal Oceanographic Bathymetry Explorer) Software . SEANOE . https://doi.org/10.17882/70460.
62. K. G. Foote, H. P. Knudsen, G. Vestnes, Calibration of Acoustic Instruments for Fish Density-Estimation - a Practical Guide. J Acoust Soc Am 83, 831-832 (1988).
63. Y. Sano, T. P. Fischer, in The noble gases as geochemical tracers. (Springer, 2013), pp. 249-317.
64. W. Aeschbach-Hertig, D. K. Solomon, Noble gas thermometry in groundwater hydrology. The noble gases as geochemical tracers, 81-122 (2013).
65. A. L. Rizzo et al., Kolumbo submarine volcano (Greece): An active window into the Aegean subduction system. Scientific Reports 6, (2016).
66. C. Tilliette et al., Dissolved Iron Patterns Impacted by Shallow Hydrothermal Sources Along a Transect Through the Tonga-Kermadec Arc. Global Biogeochemical Cycles 36, e2022GB007363 (2022).
67. M. Tonnard et al., Dissolved iron in the North Atlantic Ocean and Labrador Sea along the GEOVIDE section (GEOTRACES section GA01). Biogeosciences 17, 917-943 (2020).
68. P. Bouruet-Aubertot et al., Longitudinal contrast in turbulence along a similar to 19 degrees S section in the Pacific and its consequences for biogeochemical fluxes. Biogeosciences 15, 7485-7504 (2018).
69. T. R. Osborn, Estimates of the Local-Rate of Vertical Diffusion from Dissipation Measurements. J Phys Oceanogr 10, 83-89 (1980).
70. T. M. Dillon, Vertical Overturns - a Comparison of Thorpe and Ozmidov Length Scales. J Geophys Res-Oceans 87, 9601-9613 (1982).
71. S. A. Thorpe, Turbulence and Mixing in a Scottish Loch. Philos T R Soc A 286, 125-181 (1977).
72. E. Kunze, E. Firing, J. M. Hummon, T. K. Chereskin, A. M. Thurnherr, Global abyssal mixing inferred from lowered ADCP shear and CTD strain profiles (vol 36, pg 1553, 2006). J Phys Oceanogr 36, 2350-2352 (2006).
73. A. Aminot, R. Kerouel, Quae, Ed. (2007), pp. 187 pp.
74. S. Bonnet et al., In-depth characterization of diazotroph activity across the western tropical South Pacific hotspot of N-2 fixation (OUTPACE cruise). Biogeosciences 15, 4215-4232 (2018).
75. I. Klawonn et al., Simple approach for the preparation of 15−15N2-enriched water for nitrogen fixation assessments: evaluation, application and recommendations. Frontiers in microbiology 6, (2015).
76. M. Benavides, H. Berthelot, S. Duhamel, P. Raimbault, S. Bonnet, Dissolved organic matter uptake by Trichodesmium in the Southwest Pacific. Scientific Reports 7, 41315 (2017).
77. P. H. Moisander et al., Analogous nutrient limitations in unicellular diazotrophs and Prochlorococcus in the South Pacific Ocean. The ISME journal 6, 733-744 (2011).
78. J. P. Montoya, M. Voss, P. Kahler, D. G. Capone, A simple, high-precision, high-sensitivity tracer assay for N2 fixation. Applied and Environmental Microbiology 62, 986-993 (1996).
79. T. M. Kana et al., A membrane inlet mass spectrometer for rapid high precision determination of N2, O2, and Ar in environmental water samples. Analytical Chemistry 66, 4166–4170 (1994).
80. A. M. Moisander, A. Beinart, M. Voss, J. P. Zehr, Diversity and abundance of diazotrophs in the South China Sea during intermonsoon. The ISME journal 2, 954-967 (2008).

81. M. J. Church, B. D. Jenkins, D. M. Karl, J. P. Zehr, Vertical distributions of nitrogen-fixing phylotypes at Stn ALOHA in the oligotrophic North Pacific Ocean. Aquatic Microbial Ecology 38, 3-14 (2005).
82. K. A. Turk-Kubo et al., Diazotroph community succession during the VAHINE mesocosms experiment (New Caledonia Lagoon). Biogeosciences 12, 7435-7452 (2015).
83. P. W. Boyd, A. McDonnell, J. Valdez, D. LeFevre, M. P. Gall, RESPIRE: An in situ particle interceptor to conduct particle remineralization and microbial dynamics studies in the oceans' Twilight Zone. Limnol Oceanogr-Meth 13, 494-508 (2015).
84. M. Bressac et al., Resupply of mesopelagic dissolved iron controlled by particulate iron composition. Nature Geoscience 12, 995-+ (2019).
85. L. A. Anderson, J. L. Sarmiento, Redfield Ratios of Remineralization Determined by Nutrient Data-Analysis. Global Biogeochemical Cycles 8, 65-80 (1994).
86. C. Guieu et al., Vertical particle flux in the northeast Atlantic Ocean (POMME experiment). J Geophys Res-Oceans 110, (2005).
87. K. L. Casciotti, D. M. Sigman, M. G. Hastings, J. K. Böhlke, A. Hilkert, Measurement of the Oxygen Isotopic Composition of Nitrate in Seawater and Freshwater Using the Denitrifier Method. Analytical Chemistry 74, 4905–4912 (2002).
88. D. M. Sigman et al., A bacterial method for the nitrogen isotopic analysis of nitrate in seawater and freshwater. Analytical Chemistry 73, 4145–4153 (2001).
89. M. R. McIlvin, K. L. Casciotti, Technical updates to the bacterial method for nitrate isotopic analyses. Analytical Chemistry 83, 1850-1856 (2011).
90. F. Gazeau et al., Impact of dust addition on the metabolism of Mediterranean plankton communities and carbon export under present and future conditions of pH and temperature. Biogeosciences 18, 5423-5446 (2021).
91. M. Caffin et al., N2 fixation as a dominant new N source in the western tropical South Pacific Ocean (OUTPACE cruise). Biogeosciences 15, 2565-2585 (2018).
92. R. Alkalay et al., Carbon export and drivers in the southeastern Levantine Basin. Deep-Sea Research Part Ii-Topical Studies in Oceanography 171, (2020).
93. E. Ternon et al., The impact of Saharan dust on the particulate export in the water column of the North Western Mediterranean Sea. Biogeosciences 7, 809-826 (2010).
94. D. M. Karl et al., in Ocean Biogeochemistry: The Role of the Ocean Carbon Cycle in Global Change, Fasham, Ed. (Springer, New York, 2003), pp. 239-267.
95. M. W. Lomas, N. R. Bates, R. J. Johnson, D. K. Steinberg, T. Tanioka, Adaptive carbon export response to warming in the Sargasso Sea. Nature Communications 13, 1211 (2022).
96. D. M. Karl et al., Seasonal-to-decadal scale variability in primary production and particulate matter export at Station ALOHA. Progress in Oceanography 195, (2021).

Acknowledgments: The dataset presented here resulted from the efforts of many individuals both onboard and on land who contributed to the success of the expedition. We thank the captain and the crew of the R/V *L'Atalante* (TGIR Flotte, operated by IFREMER), in particular S. Laville Saint-Martin and J. Le Doare for their help during the multibeam survey, as well as the Technical Division INSU for the technical support and the equipment provision. We thank the captain and the crew of the R/V *Alis* (TGIR Flotte, operated by IFREMER), for the safe recovery of the fixed mooring in particularly difficult weather conditions. We thank Céline Dimier and the SAPIGH platform of the Institut de la Mer de Villefranche (IMEV) for sampling on board and performing the pigment analyses, and Mariano Tantillo for helping in the noble gas extraction from water samples and isotope analysis performed at the noble gas laboratory of INGV-Palermo. Finally, we thank Mr Lucas Jr for the English editing. Finally we are very

grateful and thank JP Gattuso, S. Blain, A. Tagliabue and L. Guidi for their advice on the manuscript. We also thank

Funding:
Agence Nationale de Recherche grant ANR-18-CE01-0016 (SB, CG)
A-Midex grant TONGA (SB, CG)
Institut National des Sciences de l'Univers Les Enveloppes Fluides et l'Environnement grant TONGA (SB, CG)
TGIR Flotte océanographique française TONGA cruise (CG, SB)
Institut de recherche pour le Développement (IRD) (SB)
MEMESTRA Grant (CB)
US NSF-OCE 1829797 (ANK)

Author contributions:
Conceptualization: SB, CG
Methodology: SB, CG, CB, FG
Investigation: SB, CG, VT, CB, FG, MB, DGS, JMG, OG, JH, CL, EP, GS, CT
Data curation: SB, CG, VT, CB, PBA, CS, FG, MB, ANK, YC, DGS, HJF, JH, NL, SN, ALR, GS, CS
Visualization: SB, CG, CB, FG, PBA, ANK, HJF
Writing – original draft: SB, CG
Writing – review & editing: All

Competing interests: Authors declare that they have no competing interests.
Data and materials availability: All data are available in the main text or the supplementary materials. The delta ^{15}N data are deposited to the BCO-DMO database https://www.bco-dmo.org/dataset/869963. The biogeochemical data are deposited on the INSU-LEFE-CYBER database http://www.obs-vlfr.fr/proof/php/TONGA/tonga_log_basicfiles.php and the acoustic data on the SEANOE database https://campagnes.flotteoceanographique.fr/campagnes/18000884/

Supplementary Materials
Materials and Methods
References (59-96)
Figs. S1 to S10
Tables S1 to S7

Figure legends.

Fig. 1. Acoustic, optical and chemical anomalies measured above Volcano #1. (A) Location map showing the Tonga volcanic arc system and Volcano #1 (V1, red triangle, -21.154; 175.744). (B) Bathymetry of Volcano #1 performed during TONGA, and position of the fluid/gas active sites detected by the multibeam echo sounder (EM710, 70-110 kHz) during the survey. The white circle represents the specific site studied here ('Panamax site'), from which the data are shown in panels C, D, E, F. (C) Multibeam echo sounder image (EM710, 70-110 kHz) showing hydrothermal gas and fluid emissions from the seafloor rising up to ~10 m below the sea surface. (D) Time series (11h) of acoustic signal detected by the sounder EK60 (38kHz) showing gas/fluid seafloor emissions at a fixed position (visualization threshold -75dB). (E) Vertical CTD profiles of temperature, pH, turbidity, and Eh in the main acoustic signal. (F) Vertical profiles of methane (CH_4, nM), dissolved Mn (nM), and dissolved Fe (nM) concentrations above Volcano #1.

Fig. 2. Chlorophyll patch in the vicinity of Tonga and associated biogeochemical and biological parameters. (A) Surface [Chl*a*] MODIS composite averaged over the time period corresponding to the TONGA cruise (1 November-6 December 2019) at a resolution of 4 km and zoom of the bloom region (~360 000 km^2). The bloom is delineated by the isoline 0.9 µg $liter^{-1}$ (corresponding to twice the average background [Chl*a*] concentration outside the bloom. (B) Monthly climatology of [Chl*a*] from a 25 years-time series (GLOBCOLOR product) at 2 sites along 20°S; the red line corresponds to the region of the Tonga bloom represented with the red dot on panel (A), and the blue line corresponds to the location of the reference site in the South Pacific Gyre, represented as a blue dot on panel (A). Horizontal and vertical distributions of (C) Total Chl*a* concentrations (µg L^{-1}), (D) Particulate organic nitrogen concentrations (µmol L^{-1}), (E) N_2 fixation rates (nmol N L^{-1} d^{-1}), (F) *Trichodesmium* abundances (Log nifH gene copies L^{-1}), (G) Dissolved Fe concentrations (nmol $liter^{-1}$). Y axis: depth (m), X axis: longitude; grey dots correspond to sampling depths at the various stations.

Fig. 3. Experimental evidence of the impact of hydrothermally-enriched water additions on diazotroph communities. Temporal evolution of (A) N_2 fixation rates (nmol N L^{-1} d^{-1}), (B) *Trichodesmium* abundances (*nifH* gene copies L^{-1}) along the 196h of the experiment in the control treatment (no fluid addition), and in the reactors amended with 1.8%, 5.5%, and 14.5% of 'plume water' collected at the 'Panamax site' of Volcano #1 (~200 m depth). Error bars correspond to standard deviations on triplicate analyses.

Fig. 4. Seasonal variability of export at 1000 m in the Fe-fertilized patch over one year (fixed mooring deployed at -20.702; -177.866 from Nov. 2019-Nov 2020; see SI)). Blue line: particulate organic carbon (POC) export fluxes (mmol C m^{-2} d^{-1}). Red line: δ15N (per mil) signature of exported PON.

Table 1. Carbon and Fe budgets in the naturally-fertilized region of the Tonga volcanic arc and the distal reference site, and comparisons with natural fertilizations in HNLC regions.

	TONGA		CROZEX (2,5)	KEOPS (2,3)
	+Fe (Volcano #1)	-Fe (Gyre)		
Bloom area (km^2)	360000	No bloom	90000	45000
Bloom duration (d)	180	-	58	75-105
Integrated Chla over the euphotic zone (mg Chl*a* m^{-2})	39	-	98.1	72-318
Vertical diffusivity (Kz, m^2 s^{-1})	$3.7 \pm 1.9 \times 10^{-5}$	$5.2 \pm 9.6 \times 10^{-6}$		
Vertical DFe gradient (mol m^{-4})	$3.1 \pm 4.7 \times 10^{-8}$	$7.8 \pm 3.1 \times 10^{-11}$		
Vertical DFe diffusive flux (mmol Fe m^{-2} d^{-1})	$1.1 \pm 1.7 \times 10^{-4}$	$3.5 \pm 3.1 \times 10^{-8}$	6.0×10^{-5}	3.1×10^{-5}
Atmospheric DFe supply (mmol Fe m^{-2} d^{-1}) (1)	2.0×10^{-5}	2.5×10^{-5}	1.0×10^{-4}	1.7×10^{-6}
Horizontal DFe supply (mmol Fe m^{-2} d^{-1})	0 (4)	0 (4)	3.9×10^{-4}	1.9×10^{-4}
Total DFe supply (mmol Fe m^{-2} d^{-1})	1.3×10^{-4}	2.5×10^{-5}	5.5×10^{-4}	2.2×10^{-4}
Total annual DFe supply (mmol Fe m^{-2})	4.7×10^{-2}	0.9×10^{-2}	20.0×10^{-2}	8.1×10^{-2}
POC export 170 m (mmol C m^{-2} d^{-1})	3.2	1.7		
POC export 270 m (mmol C m^{-2} d^{-1})	3.9	1.4		
"Excess" C sequestration efficiency Ceffx 170 m (mol C mol^{-1} Fe)	13600	-	8640	154000
"Excess" C sequestration efficiency Ceffx 270 m (mol C mol^{-1} Fe)	23000	-		

(1) Guieu et al., (2018)
(2) Morris & Charrette, (2013)
(3) Blain et al., (2007) updated by Chever et al., (2010)
(4) The main flux is from below, lateral advection is likely negligible
(5) Pollard et al., (2009)

Figure 1

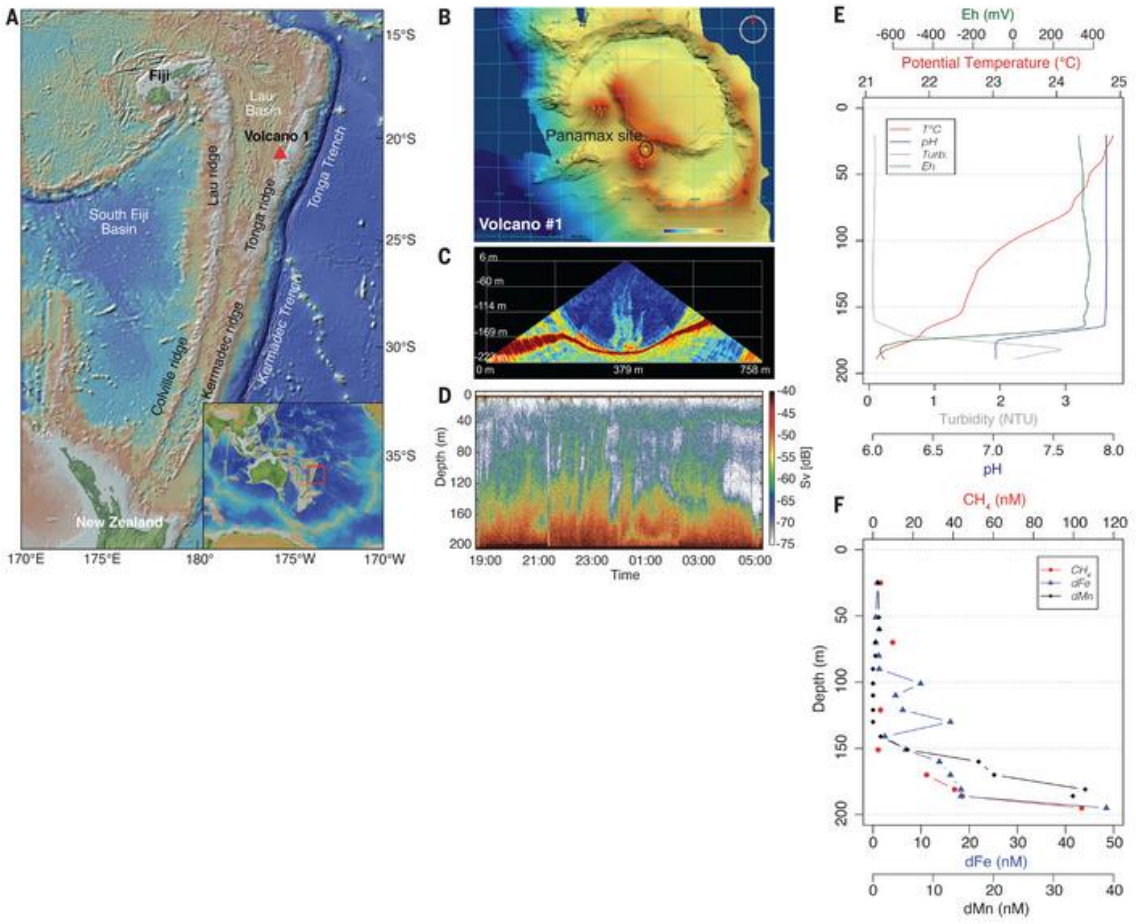
A
Fiji
Lau Basin
Volcano 1
South Fiji Basin
Lau ridge
Tonga ridge
Tonga Trench
Colville ridge
Kermadec ridge
Kermadec Trench
New Zealand
15°S
20°S
25°S
30°S
35°S
170°E
175°E
180°
175°W
170°W
B
Panamax site
Volcano #1
C
6 m
-60 m
-114 m
-169 m
-223 m
0 m
379 m
758 m
D
Depth (m)
Time
19:00
21:00
23:00
01:00
03:00
05:00
Sv [dB]
E
Eh (mV)
Potential Temperature (°C)
Turbidity (NTU)
pH
F
CH4 (nM)
Depth (m)
dFe (nM)
dMn (nM)

Figure 2

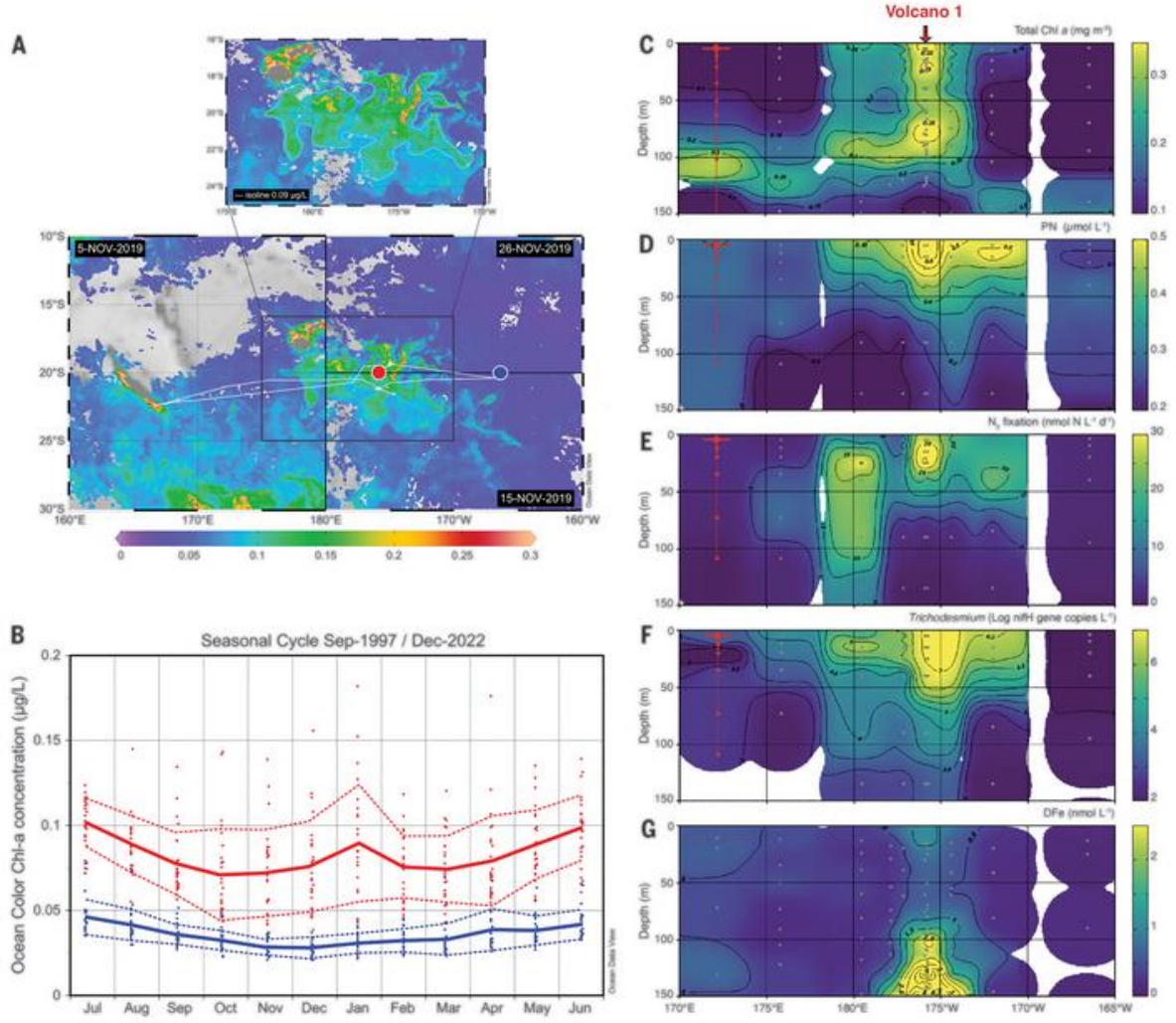

Figure 3

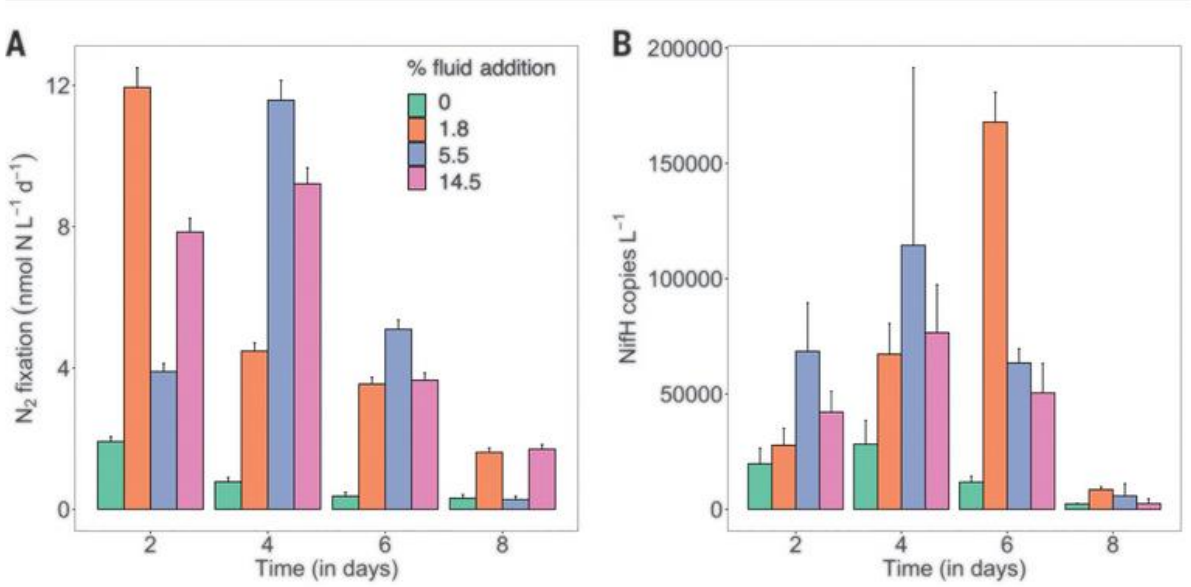

Figure 4

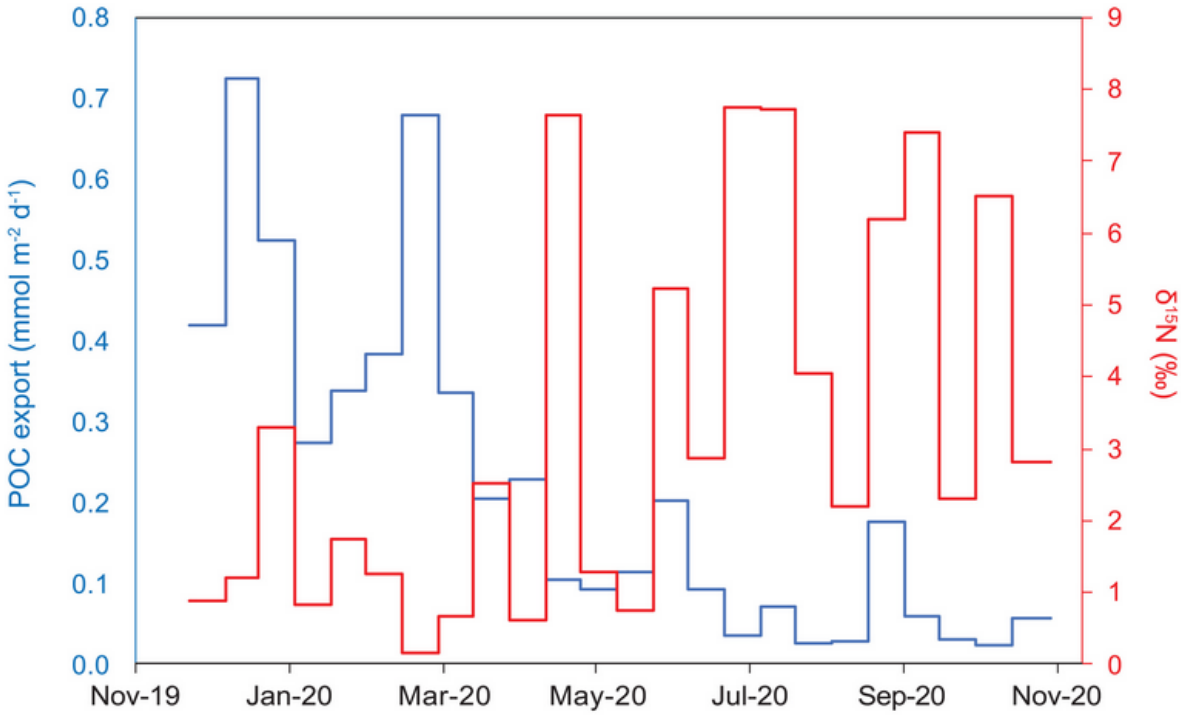
POC export (mmol m-2 d-1)
δ15N (‰)
0.0
0.1
0.2
0.3
0.4
0.5
0.6
0.7
0.8
0
1
2
3
4
5
6
7
8
9
Nov-19
Jan-20
Mar-20
May-20
Jul-20
Sep-20
Nov-20